PHYSICAL REVIEW LETTERS

Micrometric Granular Ripple Patterns in a Capillary Tube

F. Zoueshtiagh,[1] P. J. Thomas,[2] V. Thomy,[3] and A. Merlen[1]

[1]*Laboratoire de Mécanique de Lille UMR CNRS 8107, Bd Paul Langevin, 59655 Villeneuve d'Ascq, France*
[2]*Fluid Dynamics Research Centre, School of Engineering, University of Warwick, Coventry CV4 7AL, United Kingdom*
[3]*Institut d'Electronique et de Microélectronique et Nanotechnologie UMR CNRS 8520,*
Avenue Poincaré, 59652 Villeneuve d'Ascq, France

The oscillatory motion of a fluid carrying micron-sized particles inside a capillary tube is investigated experimentally. It is found that initially uniformly distributed particles can segregate and accumulate to form regularly spaced micron-sized particle clusters. The wavelength of the microclusters is compared to data for macroscale sand-ripple patterns and found to obey the same universal scaling as these. A dimensional analysis is performed that confirms the universality of the experimentally observed scaling. The experimental data for the microripple clusters further suggest the existence of a minimum particle length scale for which patterns can form and below which the Brownian motion associated with the molecules of the matrix fluid inhibits pattern formation.

Microfluidic devices are common in science and engineering, e.g., equipment for drug delivery, systems for the analysis of chemical substances [1,2] or devices for the separation of suspended microparticles, cells, or macromolecules in fluids. In these contexts observations of pattern-formation phenomena in microfluidic two-phase flows have been described [3–6]. We report a new such pattern that appears to be closely related to the well-known type of macroscopic sand-ripples [7–11] one finds on beaches or on the bottom of the ocean and rivers.

Our experimental setup, see Fig. 1, comprises a glass capillary tube (diameter $D = 288$ μm) mounted underneath a microscope and filmed with two synchronized CCD cameras A and B. Optical distortions, while filming the tube, are minimized by placing it in the water-filled gap between two parallel microscope slides. The tube is connected to a Hamilton syringe (25 μl) by means of a Teflon PTFE tube with an internal diameter of 300 μm. The whole flow circuit is fully filled with water. The capillary tube contained approximately 5 μl Duke Scientific polymer microspheres (diameter d_G: 1 or 10 μm; standard deviation from mean less than 5%; particle density $\rho_G = 1.05$ g/cm^3). Microscopic inspection revealed that the system was free of entrapped air bubbles. According to the manufacturer the concentration of the microspheres is 1.8×10^7 and 1.8×10^{10} spheres per milliliter for the 10 and the 1 μm particles, respectively.

The syringe is connected to a computer-controlled KDS syringe pump. This facilitates a continuous, alternating, linear injection and withdrawal of prescribed volumes of liquid at frequency f. This results in a reversing flow inside the capillary tube. Its amplitude, A, corresponds to the pump stroke and the smallest value is $A \approx 0.76$ mm. The mean flow velocity, V, and the amplitude of the flow motion are monitored by camera B in Fig. 1 which records the displacement of the air-liquid interface visible at the end of the capillary tube.

Video recordings of experiments with 10-μm particles revealed that ripple patterns form for certain combinations of f and A. When ripples form they are located close to the bottom in the lower half of the capillary tube. Particles suspended higher up, i.e., further away from the tube wall (closer to its center) do not appear to cluster. Patterns typically form after a few tens of seconds and settle on a stable size and wavelength after a few hundreds of seconds. Figure 2 displays two typical micro-ripple grain clusters. The patterns were not as well developed for all parameter regimes, in some cases they appeared rather faint such that clusters were hardly observable. Figure 3(a) shows a phase diagram which reveals that clear patterns were detected for $0.24 \lesssim f \lesssim 1.1$ Hz and amplitudes $A \lesssim 3$ mm. This range corresponds to the regime where most of the particles settle on the bottom of the channel. Figure 3(b) displays two typical examples illustrating the temporal development of the cluster wavelength; it initially decreases and adopts a quasistable state by about $t = 400$ s.

In Fig. 4 we use the average wavelength during the quasistable phase (diamonds) for comparison with approximately 900 experimental data points from the literature (dots) on macroscopic sand ripples forming in a number of fundamentally different experimental arrangements including unidirectional and oscillatory flows (for
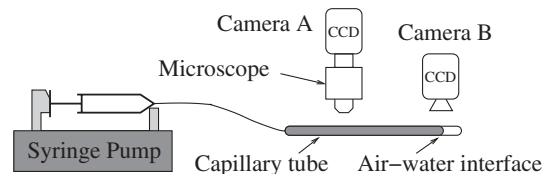

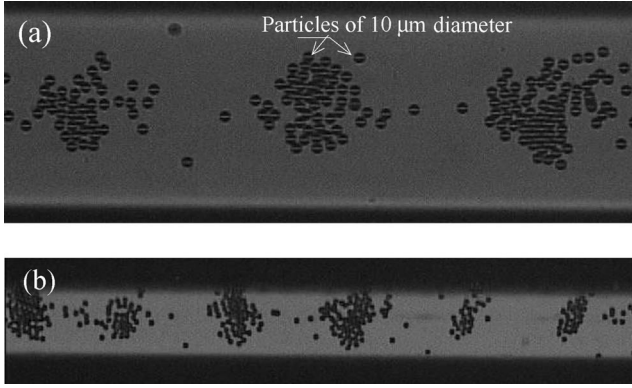FIG. 1. Sketch of the experimental setup.

FIG. 2. Example of observed patterns (a) X100 magnification (b) X50 magnification. For a video example cf. Ref. [21].

details see Ref. [12]). The pattern wavelength is nondimensionalized as (λ/d_G) and a mobility parameter Θ—similar to a Shields parameter—is defined as (compare Ref. [12]; see also [10,11,13,14])

$$\Theta = \rho_G U^2 / [g(\rho_G - \rho_F)d_G]. \qquad (1)$$

In Eq. (1), U is a typical velocity scale characterizing the flow velocity that quantifies the forcing of the system. In the present system U is identified with the speed V of the air-liquid interface as monitored by means of camera B in Fig. 1. The solid line, $\lambda/d_G = 17.64\Theta^{0.52}$, in Fig. 4 is a least-squares fit from Ref. [12] interpolating the data points of the macroscopic sand ripples. It can be clearly seen that the present data points for the microripples group around the data fit for the macroscopic sand ripples. In particular the new microripple data points extend the scaling of
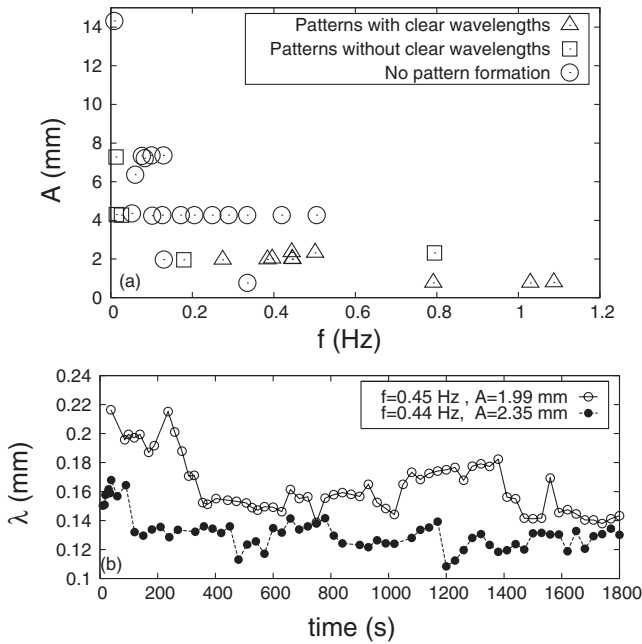

FIG. 3. (a) Phase diagram for cluster formation. (b) Ripple wavelength as a function of time.

Ref. [12] by almost 1 order of magnitude towards smaller Θ values. This suggests that the microclusters obey the same scaling one observes for macroscopic sand ripples and that they constitute an analogue to these. It is emphasized that the solid line $\lambda/d_G = 17.64\Theta^{0.52}$ in Fig. 4 represents a purely empirical result. However, we now show that the $\Theta^{1/2}$ scaling follows from a dimensional analysis.

The macroscopic sand-ripple data in Fig. 4 are generally associated with relatively large Reynolds numbers and turbulent flow conditions. The present micro clusters develop, however, in a laminar Poiseuille flow with particle Reynolds numbers as low as $\mathrm{Re} = d_G U/\nu \approx 10^{-2}$. The fact that ripple clusters do form at such low Reynolds numbers and that their wavelength appears to scale in the same manner as for flow in entirely different experiments and flow regimes prompted one of our main conclusions. It implies that the formation mechanism must be governed by local scales. Hence, global scales and global-flow features are irrelevant. Thus, one can assume that the flow at the fluid-grain interface can be characterized by a single local velocity U_L. This implies the assumption that the interface is well defined. Particles are not in suspension as can be the case, for instance, for large Af in the present experiment. The interface must also be sufficiently homogeneous such that spatial variations of U_L are negligible. We further exclude wavy interfaces with preexisting ripple structures (see Ref. [15] for the difference between wavy and plane initial interfaces).

The phenomenon is described by the equations of motion of the grains at the ripple-fluid interface accounting for all mechanical forces, such as stick-slip friction and hydrodynamic forces. Hydrodynamic forces and gravity are summarized in the Navier-Stokes equation which, with respect to boundary and initial conditions, introduces the following set of characteristic parameters:

$$[\rho_G d_G^3, \, g(\rho_G - \rho_F)d_G^3, \, \phi g(\rho_G - \rho_F)d_G^3, \, H, \, \nu, \, \rho_F, \, U_L, \, f]. \qquad (2)$$

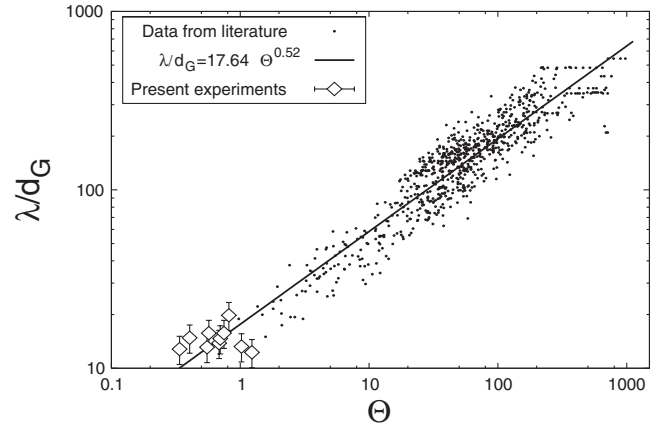The first two parameters in (2) are the mass and the

FIG. 4. Nondimensionalized ripple wavelength, λ/d_G, as a function of the mobility parameter Θ.

apparent weight of the grains. The third is the Coulomb friction force on the granular bed and ϕ represents the friction coefficient for which typical values of 0.7 are commonly quoted [16]. The fifth parameter, H, is a global length scale long enough to characterize the ripple patterns while ν is the kinematic viscosity of the fluid. Finally, f is a characteristic frequency of the oscillation or rotation. Since one can incorporate body forces (hydrostatic pressure) in the pressure term of the Navier-Stokes equation the gravity, g, will only appear in the context of the apparent mass but never independently unless free-surface effects must be accounted for. Thus, only the kinematic viscosity, ν and ρ_F appear explicitly in the Navier-Stokes equations. Note that, in practical cases, the global length H is much larger than d_G. It can therefore be used to characterize the number of grains per unit surface of the granular bed which is proportional to H^2/d_G^2. In fact, all purely geometric quantities, such as d_G, can be omitted since one characteristic length is sufficient for geometric considerations as long as all shapes remain unchanged.

Choosing H, $g(\rho_G - \rho_F)d_G^3$ and $\rho_G d_G^3$ as the primary, repeating variables for a dimensional analysis and after rearranging the dimensionless parameters that one obtains, the wavelength can be written as

$$\frac{\lambda}{H} = \mathcal{F}\left(\phi, \frac{\rho_G U_L^2}{\Delta\rho g d_G}, \frac{\nu\sqrt{\rho_G}}{\sqrt{\Delta\rho g d_G^3}}, \frac{\rho_F H^3}{\rho_G d_G^3}, \frac{\rho_G f^2 d_G}{\Delta\rho g}\right). \quad (3)$$

In Eq. (3) $\Delta\rho = \rho_G - \rho_F$ and $\mathcal{F}$ is a dimensionless function depending on the geometry of the problem (relative sizes, shapes, dimensionless dispersion of the grain sizes, etc.). While Eq. (3) highlights the role of the local velocity U_L it does not have practical use since U_L cannot be determined easily. Therefore, one has to relate U_L to the global flow with its characteristic velocity scale U ($U = V \sim Af$ in present experiment). The boundary layer, or more generally a viscous shear layer, above the sand ripples determines the average velocity gradient at the sand surface. This gradient can only be determined by global scales and its characteristic magnitude is U/H. For a boundary layer H represents a characteristic boundary-layer thickness. For the present Poiseuille flow it is equal to the radius $D/2$, of the capillary tube. Using this average velocity gradient one concludes that the magnitude of U_L, i.e., the typical velocity scale at height d_G above the granule bed, is $(U/H)d_G$. Introducing this scale for U_L into Eq. (3) yields

$$\frac{\lambda}{H} = \mathcal{F}\left(\phi, \Theta\frac{d_G^2}{H^2}, \frac{\nu\sqrt{\rho_G}}{\sqrt{\Delta\rho g d_G^3}}, \frac{\rho_F H^3}{\rho_G d_G^3}, \frac{\rho_G f^2 d_G}{\Delta\rho g}\right). \quad (4)$$

The behavior of Eq. (4) in the limit $d_G/H \to 0$, i.e., when the grain size is small compared to the global scale (boundary-layer thickness), is the relevant physical limit to be investigated. It is emphasized that it is only the behavior of the ratio d_G/H and not independently $d_G \to 0$ (no grains) or $H \to \infty$ (no ripples at macroscopic level)

that needs to be examined. Therefore, the equation must be written as $(\lambda/d_G)(d_G/H) = \mathcal{F}(\ldots)$. For $d_G/H \to 0$ the left-hand side of the equation approaches zero and the equation collapses unless both sides of the equation have the same asymptotic behavior. This implies that $\mathcal{F}$ must be asymptotically a linear function of d_G/H when this tends towards zero. Two parameters of $\mathcal{F}$, namely $\Theta d_G^2/H^2$ and $\rho_F H^3/\rho_G d_G^3$ depend on d_G/H. One of them is related, through Θ, to the global characteristic velocity, U, and represents the global-flow influence. The other is related to ρ_F which represents inertial effects associated with the flowing fluid. The corresponding two possibilities for the linear dependency are $(\lambda/d_G) \times (d_G/H) = (\rho_G d_G^3/\rho_F H^3)^{1/3}\mathcal{F}_0(\ldots)$ or $(\lambda/d_G)(d_G/H) = \Theta^{1/2}(d_G/H)\mathcal{F}_0(\ldots)$. The first case is unrealistic since Θ, and therefore the global-flow velocity U, would disappear from the problem (no flow). Furthermore, the function must also be universal and, hence, it must remain valid at Reynolds numbers as low as those encountered in the present experiments. Here, the inertial term in the Navier-Stokes equations is negligible and ρ_F can be omitted in the set (2). Hence, the only realistic, universal possibility for eliminating d_G/H is

$$\frac{\lambda}{d_G} = \Theta^{1/2}\mathcal{F}_0\left(\phi, \frac{\nu\sqrt{\rho_G}}{\sqrt{\Delta\rho g d_G^3}}, \frac{\rho_G f^2 d_G}{\Delta\rho g}\right). \quad (5)$$

Equation (5) reveals that one expects that $\lambda/d_G \propto \Theta^{1/2}$. This supports the choice of the scaling parameter Θ defined in Eq. (1) and, most importantly, it confirms the universality of the measured scaling $\lambda \propto \Theta^{0.52}$ in Fig. 4.

All data points in Fig. 4 further gather around one single line. Thus, they imply that the constant C of the interpolating line $\log(\lambda/d_G) = 0.52\log(\Theta) + C$ is the same for all flow regimes (laminar or turbulent boundary layer, laminar Poiseuille flow). This observation can also be understood on the basis of the asymptotic limit $d_G/H \to 0$. In this limit all global scales, such as for instance the shape of the channel, disappear from the problem. In other words, when U is large enough to produce ripples, and as long as $H \gg d_G$, then $\mathcal{F}_0$ will not involve any reference to global scales and, consequently, the constant C must necessarily be the same for all flow regimes. This is consistent with the disappearance of ρ_F at the asymptotic limit since in all the experiments of Fig. 4 the grains are not sensitive to inertial effects such as centrifugal forces caused by turbulent vortices. This is so either because of their weight, their near-wall location or beacuse of a low Reynolds number of the global flow.

The above dimensional analysis implicitly assumed that the particles forming the ripples are large enough not to be affected by the Brownian motion of the molecules of the matrix fluid nor by any nonmechanical forces such as van der Waals or Coulomb forces. This was evidently the case in the experiments with 10 μm microspheres in water where the clear patterns forming near the bottom of the

tube (because of gravity) obeyed the predicted scaling. The particles were not observed to spontaneously agglomerate together or stick on the walls providing further evidence of the absence of effects due to van der Waals or Coulomb forces. Experiments with the smaller 1 μm spheres revealed that even after time scales as long as 36 h no clear patterns were observed. This could be a consequence of the restrictions which the syringe pump imposes on the feasible values for f and A. However, it may alternatively indicate that around scales of 1 μm the Brownian motion of the water molecules becomes significant and suppresses ripple formation. The relative strength of convective transport to diffusive transport is characterized by the Peclet number, $P_e = (\upsilon d_G/2)/D$, where υ is a typical flow velocity (of the order of 10^{-3} m/s) and $D = (\kappa T)/(3\pi\mu d_G)$ is the Stokes-Einstein diffusion coefficient in one dimension [17] (κ: Boltzman constant, T: absolute temperature of fluid, μ: dynamic viscosity). It is found that P_e is of the order of about 10^5 and 10^3 for 10 and 1 μm microspheres, respectively. This would imply that effects due to diffusion are negligible. However, the mean-square displacement of a diffusing particle during a time interval, Δt, in each dimension, i, is given by [17] $\langle r_i^2(t)\rangle = 2D\Delta t$. For the period, τ, of the flow oscillation in our system ($0.92 \lesssim \tau \lesssim 117$ s.) one finds smallest values of r_i of the order of 0.1 and 1 μm for 10 and 1 μm-diameter particles, respectively. Consequently, diffusive displacement may be significant for the motion of the 1 μm-diameter particles and it may explain the absence of clustering for these. In that case the temperature would have to be taken into account in the set of parameters of expression (2) and the problem would no longer be purely mechanical. To explore whether pump limitations or Brownian motion is responsible for the absence of ripples for the 1 μm spheres we are developing an improved setup to enable experiments with larger f and A variations.

Rewriting the main result of Eq. (5) by using the local velocity, U_L, in the expression for Θ yields further physical insight into the significance of the $\Theta^{1/2}$ scaling, the equation becomes

$$\frac{\lambda}{H} = \frac{U_L}{\sqrt{g(1-\frac{\rho_F}{\rho_G})d_G}} \mathcal{F}_0\left(\phi, \frac{\nu\sqrt{\rho_G}}{\sqrt{\Delta\rho g d_G^3}}, \frac{\rho_G f^2 d_G}{\Delta\rho g}\right). \quad (6)$$

Equation (6) shows that the wavelength is directly proportional to a local Froude number when the size of the grains is small compared with the global scales. Hence, the problem is of purely mechanical nature and associated with a forcing with a characteristic frequency or angular frequency. The Froude number can be interpreted as a balance between lift and weight of the particles *but also* as a balance between drag and the friction on the interface—both effects being responsible for the phenomenon. The proportionality could be interpreted as follows. Drag and lift forces on small particles are proportional to the fluid velocity. Consequently, $U_L H$ characterizes the work required to lift a particle from the interface and entrain it into the outer flow. On the other hand, $\lambda\sqrt{g(1-\rho_F/\rho_G)d_G}$ corresponds to the frictional work associated with the motion of a particle from one ripple to the next. When spatial homogeneity of U_L can be assumed, both effects compete equally in the formation process of the ripples.

In terms of applications, it may be feasible to exploit the phenomenon for the development of new, alternative industrial technologies for separating particles or macromolecules from a fluid flow. This would constitute an alternative to existing flow-based separation techniques such as field-flow fractionation (see, e.g., [18]) or split-flow lateral thin cell fractionation (see, e.g., [19,20]).

[1] H. A. Stone and S. Kim, AIChE J. **47**, 1250 (2001).
[2] T. M. Squires and S. R. Quake, Rev. Mod. Phys. **77**, 977 (2005).
[3] F.-K. Tsai, J. L. Lauer, and J. L. Shohet, J. Appl. Phys. **99**, 024701 (2006).
[4] D. S. W. Lim, J. P. Shelby, J. S. Kuo, and D. T. Chiu, Appl. Phys. Lett. **83**, 1145 (2003).
[5] T. Thorsen, R. W. Roberts, F. H. Arnold, and S. R. Quake, Phys. Rev. Lett. **86**, 4163 (2001).
[6] A. Gunther and K. F. Jensen, Lab Chip **6**, 1487 (2006).
[7] R. A. Bagnold, *The Physics of Blown Sand and Desert Dunes* (Methuen, London, 1941).
[8] J. Sleath, *Sea Bed Mechanics* (John Wiley & Sons, New York, 1984).
[9] J. Best, J. Geophys. Res. **110**, F04S02 (2005).
[10] P. J. Thomas and F. Zoueshtiagh, Phil. Trans. R. Soc. A **363**, 1663 (2005).
[11] P. J. Thomas and F. Zoueshtiagh, J. Math. Eng. **57**, 317 (2006).
[12] F. Zoueshtiagh and P. J. Thomas, Phys. Rev. E **67**, 031301 (2003).
[13] F. Zoueshtiagh and P. J. Thomas, Phys. Rev. E **61**, 5588 (2000).
[14] P. J. Thomas, J. Fluid Mech. **274**, 23 (1994).
[15] T.-D. Miao, Q.-S. Mu, and S.-Z. Wu, Phys. Lett. A **288**, 16 (2001).
[16] J. Duran, *Sables, Poudres et Grains* (Eyrolles Sciences, Paris, 1997).
[17] R. F. Probstein, *Physicochemical Hydrodynamics: An Introduction* (Butterworth-Heinemann, Stoneham, MA, 1989).
[18] M. E. Schimpf, K. Caldwell, and J. C. Giddings, *Field-Flow Fractionation Handbook* (John Wiley & Sons, New York, 2000).
[19] J. C. Giddings, Separations Science Technology **20**, 749 (1985).
[20] C. B. Fuh, M. N. Myers, and J. C. Giddings, Anal. Chem. **64**, 3125 (1992).
[21] Real-time video of patterns formation is available in the EPAPS Document No. E-PRLTAO-100-003805 for an example of micrometric granular pattern formation in the capillary tube. Experimental parameters are $A = 2$ mm and $f = 0.26$ Hz. For more information on EPAPS, see http://www.aip.org/pubservs/epaps.html.